5-FU@DHA-UIO-66-NH_2 potentiates chemotherapy sensitivity of breast cancer cells through a microRNA let-7a-dependent mechanism

Jingquan Li[1], Fanghao Lu[2], Xin Shao[3], Bosen You[3]

[1]Department of Medical Oncology, Harbin Medical University Cancer Hospital, Harbin, China; [2]Department of Pathophysiology, Harbin Medical University, Harbin, China; [3]Department of Surgery, The Second Affiliated Hospital of Harbin Medical University, Harbin, China

Contributions: (I) Conception and design: J Li; (II) Administrative support: F Lu; (III) Provision of study materials or patients: J Li; (IV) Collection and assembly of data: X Shao; (V) Data analysis and interpretation: B You; (VI) Manuscript writing: All authors; (VII) Final approval of manuscript: All authors.

Correspondence to: Jingquan Li. Department of Medical Oncology, Harbin Medical University Cancer Hospital, Harbin, No. 150, Haping Road, Nangang District, Harbin 150081, China. Email: lijingquan@hrbmu.edu.cn.

Background: Drug delivery systems with magnetization facilitate the accumulation of drug at the target site. This study aimed to explore the mechanism by which docosahexaenoic acid (DHA)-modified porous metal-organic framework (MOF) UIO-66-NH_2 loads chemotherapeutic drug 5-fluorouracil (5-FU) and reduces the chemotherapy resistance of breast cancer (BC) cells.

Methods: UIO-66-NH_2 was synthesized and DHA with carboxyl end was used to modify the surface of UIO-66-NH_2. 5-FU was incorporated to UIO-66-NH_2 or DHA-UIO-66-NH_2 by a post-synthesis method. The loading and release of 5-FU by @DHA-UIO-66-NH_2 was investigated with ultraviolet (UV) spectroscopy. RT-qPCR was conducted to detect the expression of let-7a in cells. The uptake of DHA-UIO-66-NH_2 by MCF-7 BC cells was observed by confocal laser scanning microscope (CLSM). Cell counting kit-8 (CCK-8), flow cytometry, and live/dead cell staining were applied to investigate the effects of 5-FU@DHA-UIO-66-NH_2 on BC cells, and a BC mouse model was established to explore its effects on tumorigenesis. HE staining and routine blood index analysis were applied for determination of the biological safety of 5-FU@DHA-UIO-66-NH_2.

Results: 5-FU@DHA-UIO-66-NH_2 was successfully constructed and characterized. The loading amount of DHA-UIO-NH_2 for 5-FU reached 30.31%. DHA-UIO-66-NH_2 was effectively taken up by MCF-7 cells. Further, 5-FU@DHA-UIO-66-NH_2 exhibited stronger inhibitory effects on MCF-7 cell viability *in vitro* as well as tumorigenesis *in vivo* than 5-FU and 5-FU@UIO-66-NH_2. DHA up-regulated let-7a to reduce the resistance of MCF-7 cells to 5-FU. Moreover, the biosafety of 5-FU@DHA-UIO-66-NH_2 was identified.

Conclusions: 5-FU@DHA-UIO-66-NH_2 increased the level of let-7a in BC cells, repressed cell viability and augmented apoptosis, and thus reduced the chemotherapy resistance of BC cells.

Keywords: Breast cancer (BC); chemotherapy resistance; metal-organic framework (MOF); UIO-66-NH2; 5-fluorouracil (5-FU)

Submitted Oct 15, 2021. Accepted for publication Dec 15, 2021.
doi: 10.21037/atm-21-5978
View this article at: https://dx.doi.org/10.21037/atm-21-5978

Introduction

Breast cancer (BC) represents the most common cancer and the leading cause of cancer-specific death among women worldwide (1). 5-fluorouracil (5-FU), first introduced as a synthesized anticancer agent several decades ago, continues to be widely used for the treatment of a variety of common malignancies, including BC (2). However, like other conventional agents used in chemotherapy, 5-FU shows various disadvantages such as poor bioavailability and great non-productive drug distribution as a result of the lack of specificity for tumors (3). Due to the non-selectively, 5-FU has been reported to cause adverse side effects, serious drug resistance, and limited concentration at the target location (4). Herein, the construction of novel drug delivery system for 5-FU is of great significance in regard of improving its performance in BC.

Metal-organic frameworks (MOFs), also known as porous coordination polymers, are highly crystalline materials composed of organic linkers and metal clusters (5). As a new class of materials characterized by high specific surface areas and defined structures, MOFs are recognized as promising precursors for preparing drug delivery systems (6). Among MOFs, UIO-66-NH_2 is a zirconium-based type that has been highlighted for its low cytotoxicity and relatively high biocompatibility (7). More importantly, the amine on UIO-66-NH_2 contributes to the feasibility of post-modifying UIO-66-NH_2 to construct multifunctional MOFs, which may overcome the limitations of functional simplicity and be applied for drug delivery (8).

Docosahexaenoic acid (DHA) refers to a highly unsaturated fatty acid and is indispensable for human body, and the critical role of DHA has been recognized in maintaining normal physiological activity of nerve cells (9,10). Intriguingly, a previous study has indicated that DHA can up-regulate the expression of let-7a, thereby increasing the sensitivity of BC cells to 5-FU (11). Meanwhile, accumulating evidence has highlighted that 5-FU and DHA can upregulate the expression of let-7a in BC cells and BC cell-derived exosomes, respectively, and inhibit the occurrence and development of BC (12-14). Besides, the low-pH microenvironment in cancer tissues has revealed the potential of novel pH-sensitive drug delivery systems, for which DHA serves as a promising modifier (15). Taken together, in the present study, we synthesized DHA-modified UIO-66-NH_2 to evaluate its effectiveness as a carrier of 5-FU in BC treatment and hypothesized that 5-FU-incorporated DHA-UIO-66-NH_2 (5-FU@DHA-UIO-66-NH_2) reduce the resistance of BC cells to 5-FU by up-regulating the level of let-7a. Although there is literature reporting the effects of magnetic DHA on tumor cells (16), in this study, MOFs were used as drug carriers different from the Fe_3O_4 liposome nanomaterials as drug delivery media used in the literature. Due to the ultrahigh surface area and porosity of MOFs, the 5-FU drug loading capacity can be greatly increased; in addition, MOFs were modified with DHA and loaded with 5-FU drugs, which can play a synergistic effect in the treatment of BC. We present the following article in accordance with the ARRIVE reporting checklist (available at https://dx.doi.org/10.21037/atm-21-5978).

Methods

Ethical statement

Animal experiments were approved by the Animal Ethics Committee of Harbin Medical University Cancer Hospital (approval number: 2019-185) and performed according to the Guide for the Care and Use of Laboratory animals published by the US National Institutes of Health. Extensive efforts were made to ensure minimal suffering of the animals used in the study.

Preparation of 5-FU-incorporated DHA-UIO-66-NH_2 (5-FU@DHA-UIO-66-NH_2)

For the synthesis of UIO-66-NH_2 framework, 0.125 g ZrCl4 and 0.123 g BDC-NH2 were added to the mixed solution of 1 mL HCl and 15 mL N, N-dimethylformamide (DMF), followed by 4-h heating and stirring at 80℃. Then, for the preparation of DHA-UIO-66-NH_2, DHA and UIO-66-NH_2 were dissolved in 20 mL of DMF at different ratios (0, 1/8, 1/4, and 1/2), followed by stirring at room temperature for one day. Prepared DHA-UIO-66-NH_2 was washed with DMF to remove uncombined DHA. Subsequently, for the construction of 5-FU@DHA-UIO-66, 20 mg of 5-FU (dissolved in 20 mL PBS) was added with 5 mg DHA@UIO-66-NH_2 and stirred for 24 h in the dark.

Characterization of 5-FU@DHA-UIO-66

The morphology of 5-FU@DHA-UIO-66 was observed under a scanning electron microscope (SEM, Zeiss Field Emission SEM Supra55VP, Oberkochen, Germany). Fourier transform infrared (FT-IR) spectroscopy was performed using a Spectrum100 FT-IR spectrometer (4000–400 cm^{-1}). Powder X-ray diffraction (PXRD) data

were collected with a DX-2700B diffractometer (Dandong Haoyuan Instrument, Dandong, Liaoning, China) in the range of 5–50° (2θ) at a scan rate of 5°/min. Further, thermogravimetric analysis (TGA) was conducted under nitrogen utilizing a TGA/SDTA 851e analyzer (Mettler-Toledo, Highstown, NJ, USA) with the temperature rising from ambient temperature to 800 ℃ at a heating rate of 10 ℃/min.

5-FU@DHA-UIO-66 was also subjected to ultraviolet (UV)-VIS spectroscopy utilizing a UV-3010 spectrophotometer (Hitachi, Tokyo, Japan). The solid-state 13C MAS NMR spectrum was recorded utilizing a contact time of 3 milliseconds on a Bruker AM-400 (400 MHz) spectrometer equipped with a 5.0 mm chemical probe (Bruker Daltonik GmbH, Bremen, Germany). The nitrogen adsorption-desorption isotherm was measured with a Autosorb AS-6B/IQ2 apparatus (Quantachrome Instruments, Boynton Beach, FL, USA) under nitrogen (77 K). Moreover, the concentration of 5-FU was measured utilizing UV-VIS spectroscopy.

Loading and release of 5-FU

The loading amount of 5-FU in DHA-UIO-66-NH_2 was calculated based on the determination of the concentration of 5-FU in the solution and supernatant at different time points by UV-3010 spectrophotometer (Hitachi). The release rate of 5-FU in PBS (pH =7.4 or 5.5) was measured by dialysis. Briefly, 200 μg 5-FU@DHA-UIO-66-NH_2 was dispersed in 20 mL of PBS and subjected to dialysis (37±1 ℃, 110 rpm). At different time points during the dialysis, 1 mL of the sample was taken from the supernatant for UV detection of 5-FU content, and 1 mL of fresh PBS was simultaneously added to the original system.

Cellular uptake

The uptake of constructed MOFs by MCF-7 human BC cells was observed with confocal laser scanning microscope (CLSM). MCF-7 cells (5×10^4 per well) were first seeded on 6-well plates and incubated for 12 h, and then incubated with 10 μg/mL FITC-DHA-UIO-66-NH_2 or FITC-UIO-66-NH_2 for 0.5, 1, 3 or 6 h, followed by PBS washing. After that, the cells were fixed with 2.5% formaldehyde at 37 ℃ for 10 min, treated with DAPI (20 μg/mL in PBS) for 10 min to stain the nucleus, and observed with CLSM (Leica TCS SP8, Leica, Buffalo, NY, USA).

3-(4,5-dimethylthiazol-2-yl)-2, 5-diphenyltetrazolium bromide (MTT) assay

The biocompatibility and cytotoxicity of 5-FU@UIO-66-NH_2 and 5-FU@DHA-UIO-66-NH2 in MCF-7 cells were examined utilizing MTT assay. The cells were cultured in plates (100,000 strains per well) for 24 h (37 ℃, 5% CO_2) and transferred to new plates (100 μL medium/well). Subsequently, the cells were incubated for 48 h with 0, 0.195, 0.39, 0.781, 1.562, 3.125, 6.25, 12.5, 25, 50 and 100 μg/mL^{-1} 5-FU drugs: 5-FU@UIO-66-NH_2 or 5-FU@DHA-UIO-66-NH_2. After 48 h, the cells were incubated with 20 μL of MTT solution (5.0 mg/mL). After the supernatant removed and 150 μL of DMSO added, the optical density (OD) of the substance in each well at 570 nm was determined, and the data were characterized by the mean value ± standard deviation (SD).

Cell viability detection

MCF-7 cells cultured in 96-well plates (5×10^4 cells/well) were incubated with 5-FU@UIO-66-NH_2 or 5-FU@DHA-UIO-66-NH_2 of different concentrations (0.195, 0.39, 0.781, 1.562, 3.125, 6.25, 12.5, 25, 50 and 100 μg/mL) for 24 h. Then, the inhibiting effects of the drug on MCF-7 cell viability were detected by trypan blue staining of viable cells.

Flow cytometry

Cell apoptosis was detected following the protocols of Annexin V-fluorescein isothiocyanate (Annexin V-FITC)/propidium iodide (PI) counterstaining kit (BD Biosciences, San Diego, CA, USA). Briefly, MCF-7 cells (upon cell confluence reaching 70%) were incubated with 10 μg/mL 5-FU@UIO-66-NH_2 or 5-FU@DHA-UIO-66-NH_2 for 48 h, digested with EDTA-free trypsin, and stained by Annexin V-FITC and PI, followed by detection using a flow cytometer (BD FACSVerse, BD Biosciences, Bedford, MA, USA) with an excitation wavelength of 488 nm and an emission wavelength of 525 nm.

Live/dead cell staining

MCF-7 cells were cultured overnight in 8-well plates (3×10^4 cells/well) and then incubated for 24 h with 5-FU@UIO-66-NH_2 or 5-FU@DHA-UIO-66-NH_2 at a concentration of 10 μg/mL. Following that, the cells were stained with Calcein (final concentration of 2 μM) and PI

(50 μg/mL) for 10 min and then subjected to CLSM observation.

Cell transfection

MCF-7 cells and MCF7 sublines resistant to cisplatin (MCF-7/DDP) were incubated in high-sugar DMEM medium (DMEM: FBS =9:1) supplemented with 1% antibodies against streptomycin and penicillin. For transfection, plasmids expressing let-7a mimic or let-7a inhibitor, or corresponding negative control (NC) were commercially constructed (RIBOBio, Guangzhou, Guangdong, China). The cells in the logarithmic growth phase were digested, centrifuged, mixed with 1 mL of prepared culture medium, and then counted. The cells were seeded into 24-well plates (2.5×10^5 cells/well) and cell transfection was conducted when the cell confluence reached 70%. Entraster-R4000 dilution was prepared by mixing 1 μL of Entraster-R4000 with 24 μL of serum-free medium to reach a final volume of 25 μL, allowed to stand at room temperature for 5 min, and added with the aforementioned plasmids to a final volume of 50 μL for transfection.

Total RNA extraction from cells

The Eppendorf tube and other materials used for RNA extraction were cooled before the assay, and total RNA was extracted from the cells following the protocols of Trizol reagent (Invitrogen, Carlsbad, CA, USA). The concentration and purity of the extracted total RNA was determined utilizing a microplate reader.

miRNA reverse transcription

The reagents and samples involved were placed on ice, and miRNA reverse transcription was performed on ice. The reaction system of reverse transcription is shown in Table S1. After centrifugation (42 ℃, 60 min) and degeneration under 95 ℃ for 3 min, miRNA reverse transcription was terminated at 4 ℃. Prepared cDNA was immediately subjected to polymerase chain reaction (PCR) or labeled and stored at –20 ℃ for subsequent experiments.

mRNA reverse transcription

mRNA reverse transcription was also performed on ice, and the reaction system is listed in Tables S2,S3. The first reaction was terminated at 4 ℃ following a 5-min centrifugation at 65 ℃. For the second reaction, centrifugation was performed at 42 ℃ for 60 min and the reaction was terminated at 4 ℃.

miRNA quantification

The primers used for PCR was synthesized by RIBOBio (Guangzhou, Guangdong, China), shown in Table S4. SYBR Green was selected for fluorescent staining. The assay was carried out on ice without direct lighting, and the reaction system is shown in Table S5. Prepared reaction system was determined based on the protocols of the PCR kit, with U6 serving as the housekeeping gene. Then, $2^{-\Delta\Delta CT}$ method was utilized to calculate the relative expression level of the target gene.

Cell Counting Kit-8 (CCK-8) assay

Cells in the logarithmic growth phase were digested, centrifuged, and seeded onto 96-well plates (3,000 cells/well, 100 μL medium/well) for 24-h incubation (37 ℃, 5% CO_2), followed by liposome transfection of plasmids expressing let-7a mimic or inhibitor or corresponding NC. Three repeated wells were set for each group. After 24 hours of transfection, cells of each group were treated with 5-FU of different concentrations (3, 6, 12, 24, 48 μM) for 24 h. After that, CCK- 8 assay was performed to assess the inhibiting effects of 5-FU on cell viability. A microplate reader was employed to measure OD at 450 nm, and the half-maximal inhibitory concentration (IC_{50}) of 5-FU was calculated.

Establishment of a nude mouse model of BC

A BC mouse model was established to observe the anti-tumor effects of 5-FU-DHA-UIO-66-NH_2 *in vivo*. Nude mice with xenografted tumors were then classified into four groups, a Control group and other three groups subjected to treatment of 5-FU or 5-FU@UIO-66-NH_2 or 5-FU@DHA-UIO-66-NH_2. Briefly, when the tumor volume reached 300 mm^3, 100 mL of normal saline (for the Control group), 5-FU, 5-FU@UIO-66-NH_2, or 5-FU@DHA-UIO-66-NH_2 solution were injected into mice through the tail vein. The volume of xenografted tumors was measured with a caliper every three days. The administered dose of 5-FU was 5 mg/kg (17).

Biosafety assessment of 5-FU@DHA-UIO-66-NH2

To evaluate the biosafety of 5-FU@DHA-UIO-66-NH_2,

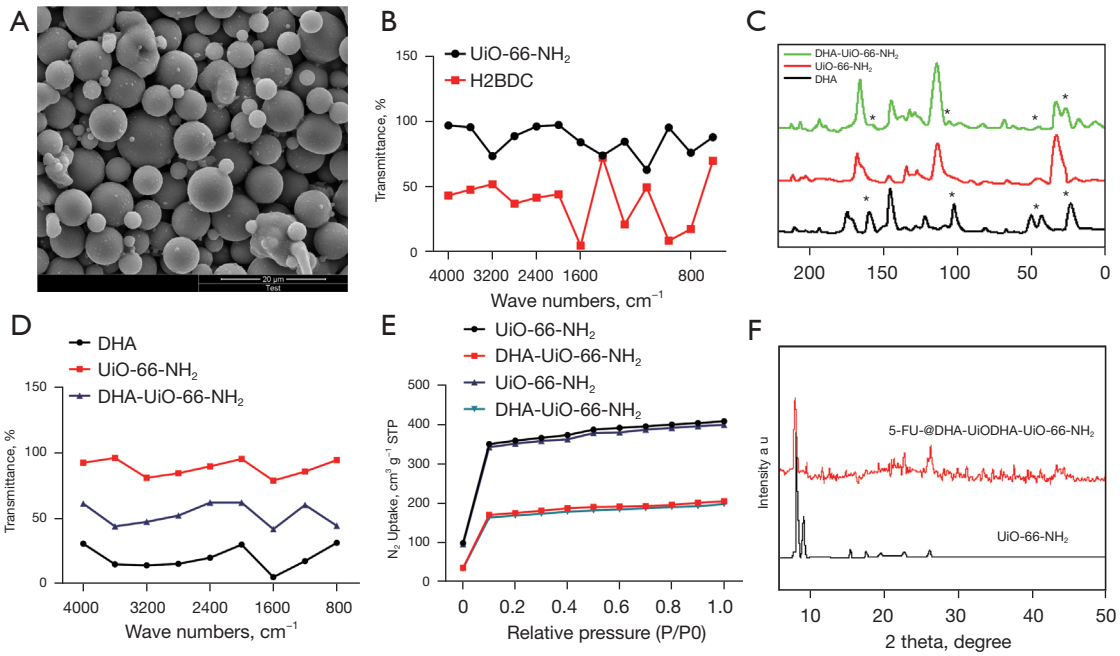

Figure 1 Construction and characterization of UIO-66-NH_2, DHA-UIO-66-NH_2, and 5-FU@DHA-UIO-66-NH_2. (A) SEM images of UIO-66-NH_2 (×10,000); (B) infrared spectrum of UIO-66-NH_2 and H_2BDC ligand; (C) NMR spectrum of UIO-66-NH_2; (D) infrared spectrum of DHA, UIO-66-NH_2 and DHA-UIO-66-NH_2 infrared spectrum; (E) adsorption and desorption curves of UIO-66-NH_2 and DHA-UIO-66-NH_2 under nitrogen (77 k); (F) PXRD pattern of DHA-UIO-66-NH_2 and 5-FU@DHA-UIO-66-NH_2. Each experiment was repeated three times. * indicates the characteristic peak of DHA. DHA, docosahexaenoic acid; 5-FU, 5-fluorouracil; SEM, scanning electron microscope; NMR, nuclear magnetic resonance; PXRD, powder X-ray diffraction.

100 μL of PBS or 5-FU@DHA-UIO-66-NH_2 (5 mg/kg 5-FU) was injected through tail vein into BALB/c nude mice, which were sacrificed 7 days later to collect major organs (heart, liver, spleen, lung and kidney). Collected organs were fixed in 4% paraformaldehyde, dehydrated with ethanol of different concentrations (50%, 70%, 90%, and, 100%), permeabilized with xylene, and embedded in paraffin. Then, the sections were subjected HE staining, followed by observation with a microscope (BX53, Olympus, Tokyo, Japan). Besides, blood cell counting and analysis of serum biochemical parameters were performed on the 1st and 7th day after the intravenous injection of 5-FU@DHA-UIO-66-NH_2.

Statistical analysis

Data in this study were processed using SPSS v.21.0 software (IBM, Armonk, NY, USA). Measurement data were summarized as mean ± SD. Unpaired *t*-test was applied to compare data of two groups. One-way analysis of variance (ANOVA) with Tukey's *post-hoc* test was performed to compare data of multiple groups. Tumor volume and weight at various time points were compared by repeated measures ANOVA with Bonferroni's *post-hoc* test. Survival rate at different time points was analyzed by two-way ANOVA. Moreover, $P<0.05$ indicated statistically significant difference.

Results

Successful construction and characterization of UIO-66-NH_2, DHA-UIO-66-NH_2, and 5-FU@DHA-UIO-66-NH_2

We synthesized UIO-66-NH_2 through hot solvent diffusion method and then DHA-UIO-66-NH_2 and 5-FU@DHA-UIO-66-NH_2. Then, SEM characterization revealed that the particle size of UIO-66-NH_2 was about 100 nm when the molar ratio of zirconium metal salt to ligand was 0.125:0.123 (*Figure 1A*). FT-IR spectroscopy of the prepared UIO-66-NH_2 indicated an obvious red shift of carboxyl functional group, identifying that the metal ion

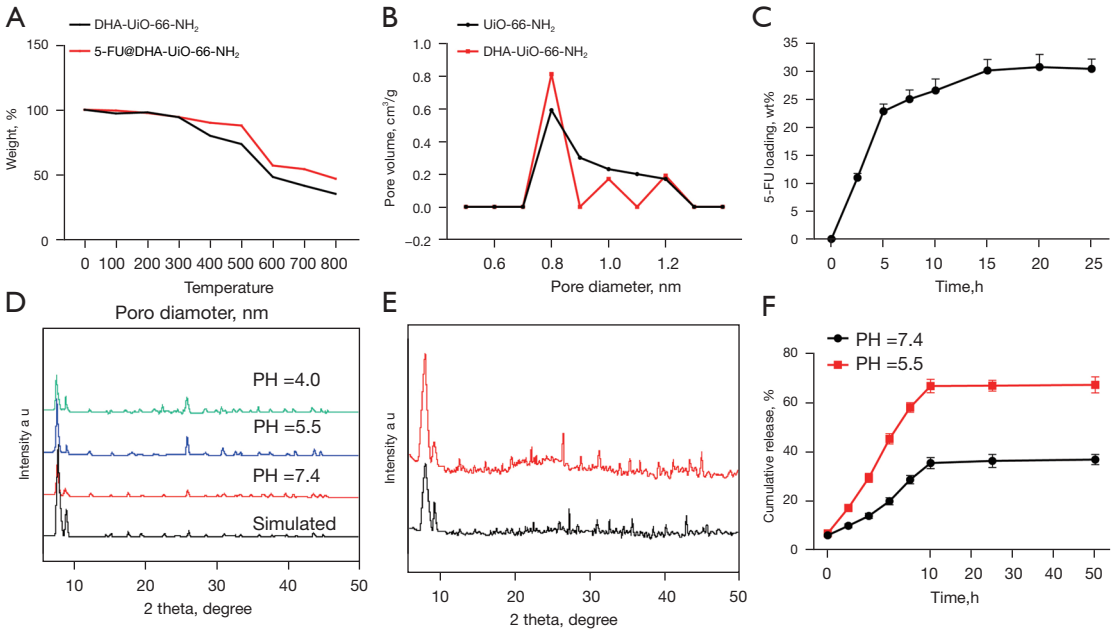

Figure 2 Thermal stability as well as 5-FU loading and release of DHA-UIO-66-NH_2. (A) Thermogravimetric curve of DHA-UIO-66-NH_2 and 5-FU@DHA-UIO-66-NH_2; (B) pore size distribution of UIO-66-NH_2 and DHA-UIO-66-NH_2; (C) 5-FU loading rate on DHA-UIO-66-NH_2; (D) water stability of 5-FU@DHA-UIO-66-NH_2; (E) material stability detected by PXRD test after three rounds of drug release; (F) the drug release rate of 5-FU in solution of pH =5.5 or 7.4. Each experiment was repeated three times. 5-FU, 5-fluorouracil; DHA, docosahexaenoic acid; PXRD, powder X-ray diffraction.

had been successfully combined with the ligand (*Figure 1B*).

Subsequently, DHA was modified to the surface of UIO-66-NH_2, and the carboxyl group at the end of DHA allow it to easily bind to UIO-66-NH_2 that has many metal clusters and aminated ligands on the surface can easily bind to the metal clusters and amino ligands on the surface of the nano-MOF. Constructed DHA-UIO-66-NH_2 was then characterized by FT-IR, PXRD, solid-state NMR, and gas adsorption. The characteristic peak of DHA appeared on the NMR spectrum of DHA-UIO-66-NH_2, showing successfully combination of DHA and UIO-66-NH_2 (*Figure 1C*). FT-IR spectrum DHA-UIO-66-NH_2 also displayed the absorption peak of DHA (*Figure 1D*), and the nitrogen gas absorption (BET) of DHA-modified UIO-66-NH_2 was lower than that of newly synthesized UIO-66-NH_2 (*Figure 1E*). Moreover, PXRD pattern of 5-FU@DHA-UIO-66-NH_2 and UIO-66-NH_2 showed no obvious differences, indicating that the framework remained intact (*Figure 1F*). Collectively, these results demonstrated the successful construction of UIO-66-NH_2, DHA-UIO-66-NH_2, and 5-FU@DHA-UIO-66-NH_2.

DHA-UIO-66-NH_2 framework effectively loads 5-FU

Following the construction of 5-FU@DHA-UIO-66-NH_2, we explored the loading of 5-FU by DHA-UIO-66-NH_2. Results of TGA uncovered decreased thermal stability of DHA-UIO-66-NH_2 as compared with 5-FU@DHA-UIO-66-NH_2 when the temperature reached 480 ℃ (*Figure 2A*). Then, the pore size of the MOFs was found to be mainly distributed in the range of micropores (0.5–1.5 nm) and slightly in the range of mesopores (1.5–3 nm), and the pore size of DHA-modified UIO-66-NH_2 was smaller than that of UIO-66-NH_2 (*Figure 2B*). Further, loading capability of 5-FU was tested in PBS, and the loading amount of DHA-UIO-NH_2 for 5-FU was 30.31% (*Figure 2C*). Moreover, 5-FU@DHA-UIO-66-NH_2 existed stably for 24 hours in the solution of pH from 4 to 7, showing good water stability (*Figure 2D*).

Furthermore, the 5-FU-carrying DHA-UIO-66-NH_2 framework remained stable even after three rounds of drug release (*Figure 2E*). Considering the nearly neutral pH value in normal human cells and the acidic condition in

tumor cells, we detected drug release under the conditions of pH 5.5 and pH 7.4. Approximately 37% of 5-FU was released from DHA-UIO-66-NH_2 under pH 7.4 and 62–75% was released under pH 5.5 (*Figure 2F*). In other words, the release of drugs was augmented by the weak acid microenvironment of the tumor. Taken together, our data suggested that DHA-UIO-66-NH_2 effectively loaded 5-FU and that 5-FU release may be promoted in tumors.

DHA-UIO-66-NH_2 and UIO-66-NH_2 particles can be effectively endocytosed by BC cells

Subsequently, we incubated MCF-7 cells with FITC-labeled DHA-UIO-66-NH_2 or UIO-66-NH_2 to observe the uptake of the two MOFs by MCF-7 cells. In the first 0.5 h, the cells presented with no obvious green fluorescence, indicating that only a few DHA-UIO-66-NH_2 or UIO-66-NH_2 were endocytosed. With the incubation time extending to 3 and 6 h, stronger FITC green fluorescence was observed in the cytoplasm and nucleus, suggesting that more MOFs penetrated the membrane and entered the cells (*Figure 3A,3B*). Hence, DHA-UIO-66-NH_2 and UIO-66-NH_2 particles were effectively endocytosed by MCF-7 BC cells.

5-FU@DHA-UIO-66-NH_2 represses the proliferation of BC cells and augments the apoptosis

Following cellular uptake, we then explored the cytotoxicity of these 5-FU-carrying MOFs. After treatment with UIO-66-NH_2, 5-FU@UIO-66-NH_2 and 5-FU@DHA-UIO-66-NH_2 of different concentrations separately, the cell viability of MCF-7 cells was measured by MTT. According to the results, the concentration of 5-FU@UIO-66-NH_2 and 5-FU@DHA-UIO-66-NH_2 was linearly related to the cell viability of MCF-7 cells, and 5-FU@DHA-UIO-66-NH_2 showed greater cytotoxicity relative to 5-FU@UIO-66-NH_2 (*Figure 4A,4B*). This may be explained from two aspects: DHA may increase the ability of the MOF to penetrate through the cell membrane; the drug can be released more effectively by DHA-modified MOF into MCF-7 cells.

Then, the morphology and viability of the cells treated with 5-FU@DHA-UIO-66-NH_2 were evaluated by optical microscopy. As shown in *Figure 4C*, cell viability of MCF-7 cells was reduced in response to 24-h treatment with 3.125 μg/mL of 5-FU@DHA-UIO-66-NH_2. Co-incubation with 5-FU or 5-FU@UIO-66-NH_2 alone also led to decreased MCF-7 cell viability, but not as obvious as that of 5-FU@DHA-UIO-66-NH_2.

In addition, we employed flow cytometry to assess the effects of 5-FU@DHA-UIO-66-NH_2 on MCF-7 cell apoptosis. After 12-h co-incubation, the cells presented with the highest apoptotic rate in response to 5-FU@DHA-UIO-66-NH_2 as compared with 5-FU or 5-FU@UIO-66-NH_2 (*Figure 4D*). Further, stronger red fluorescence was observed after 5-FU@DHA-UIO-66-NH_2 treatment versus 5-FU@UIO-66-NH_2, indicating that most MCF-7 cells had been killed by 5-FU@DHA-UIO-66-NH_2; in contrast, cells of the control group and cells treated with UIO-66-NH_2 showed strong green fluorescence, showing that most of the cells were still alive (*Figure 4E*). In summary, 5-FU@DHA-UIO-66-NH_2 exhibited stronger inhibiting effects on BC cell viability as well as stimulative effects on BC cell apoptosis.

5-FU@DHA-UIO-66-NH_2 up-regulates let-7a to reduce the resistance of BC cells to 5-FU

Further to explore the downstream mechanisms, we determined the expression of let-7a in MCF-7 cells with different treatments. The level of let-7a in MCF-7 cells in response to 5-FU@DHA-UIO-66-NH_2 (1.000±0.131) was observed to be higher than that in 5-FU@UIO-66-NH_2-treated cells (0.398±0.045), and the latter was higher than that in UIO-66-NH_2-treated cells (0.226±0.031) (*Figure 5A,5B*).

To investigate the role of let-7a in BC cell resistance, we performed functional assays and unraveled that let-7a overexpression led to reduced survival rate of 5-FU-treated MCF-7/DDP cells and let-7a inhibition led to the opposite (*Figure 5C,5D*). Moreover, our data indicated that the IC_{50} of 5-FU against MCF-7/DDP cells was decreased in the presence of let-7a mimic (10.82±0.53) relative to mimic NC (23.55±0.92), and increased in response to let-7a inhibitor (339.3±2.60) to inhibitor NC (13.15±0.86) (*Figure 5E*). Collectively, these results demonstrated that 5-FU@DHA-UIO-66-NH_2 up-regulated the level of let-7a to reduce the resistance of BC cells to 5-FU.

5-FU@DHA-UIO-66-NH_2 attenuates tumorigenesis and increases chemosensitivity in BC cells in vivo

After the aforementioned *in vitro* assay, we then evaluated the anti-tumor effects of 5-FU@DHA-UIO-66-NH_2 *in vivo*. Compared with BC mice of the control group

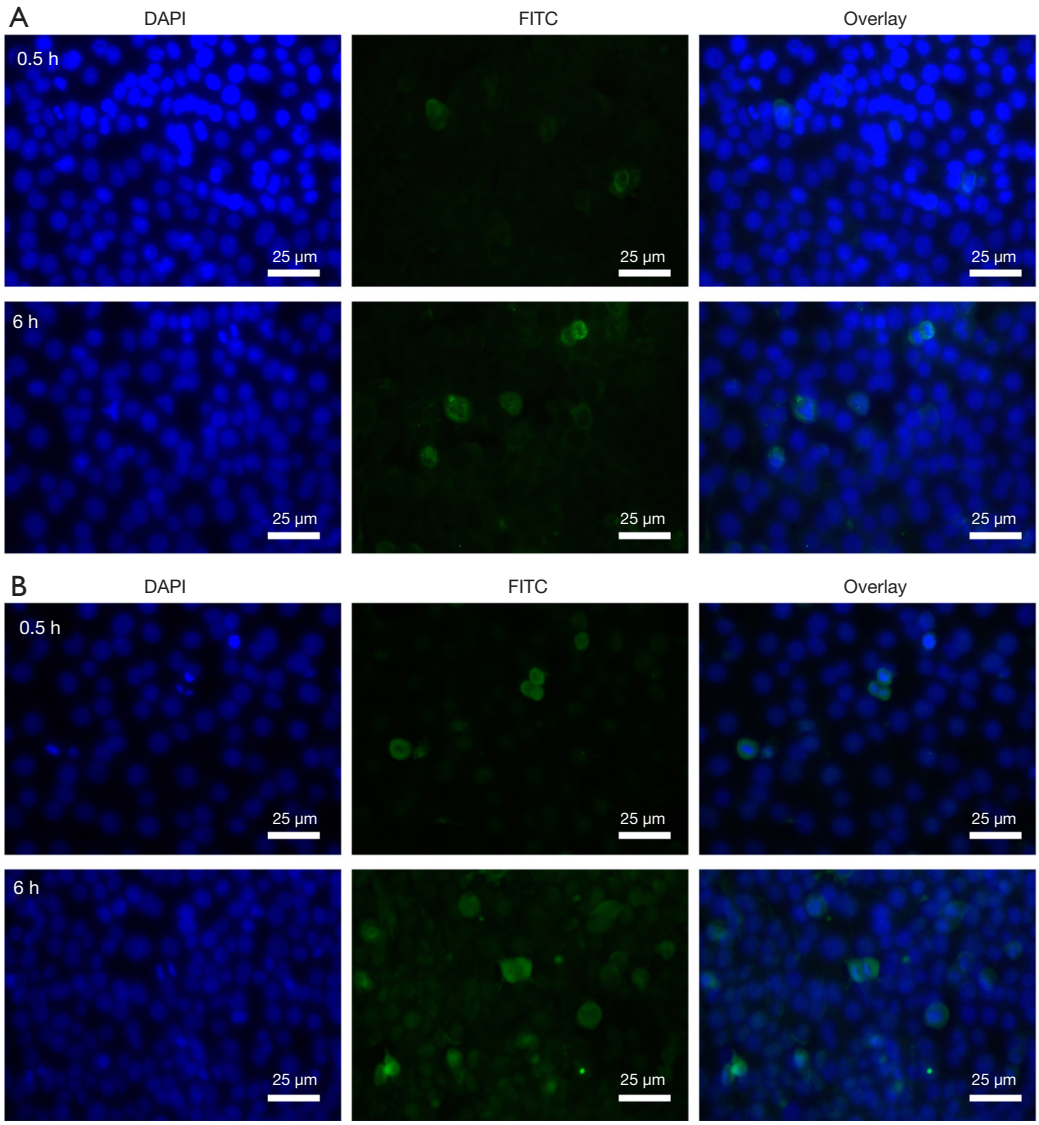

Figure 3 The uptake of DHA-UIO-66-NH_2 and UIO-66-NH2 by MCF-7 cells. (A) Representative images of CLSM of MCF-7 cells incubated with FITC-DHA-UIO-66-NH_2 at 37 ℃ for 0.5, 1, 3, and 6 h. Green fluorescence, staining of FITC-DHA-UIO-66-NH_2; blue fluorescence, staining of nuclei; (B) representative images of CLSM of MCF-7 cells incubated with FITC-UIO-66-NH_2 at 37 ℃ for 0.5, 1, 3, and 6 h. Green fluorescence, staining of FITC-UIO-66-NH_2; blue fluorescence, staining of nuclei. Each cellular experiment was repeated three times. DHA, docosahexaenoic acid; CLSM, confocal laser scanning microscope.

(treated with saline), those treated with 5-FU, 5-FU@UIO-66-NH_2 or 5-FU@DHA-UIO-66-NH_2 exhibited repressed tumorigenesis, as reflected by reduced volume of xenografted tumors within 25 days (*Figure 6A*). Besides, the body weight of the BC mice in all groups showed similar rate of rise throughout the 25 days following drug administration (*Figure 6B*). Of note, the inhibiting effects on tumorigenesis of 5-FU@UIO-66-NH_2 was stronger than that of 5-FU alone (corresponding to diminished weight of xenografted tumors), while 5-FU@DHA-UIO-66-NH_2 exerted the strongest tumor-inhibiting effects (*Figure 6C,6D*). Taken together, our data revealed that 5-FU@DHA-UIO-66-NH_2 effectively suppressed the tumorigenic ability of BC cells in nude mice and enhanced

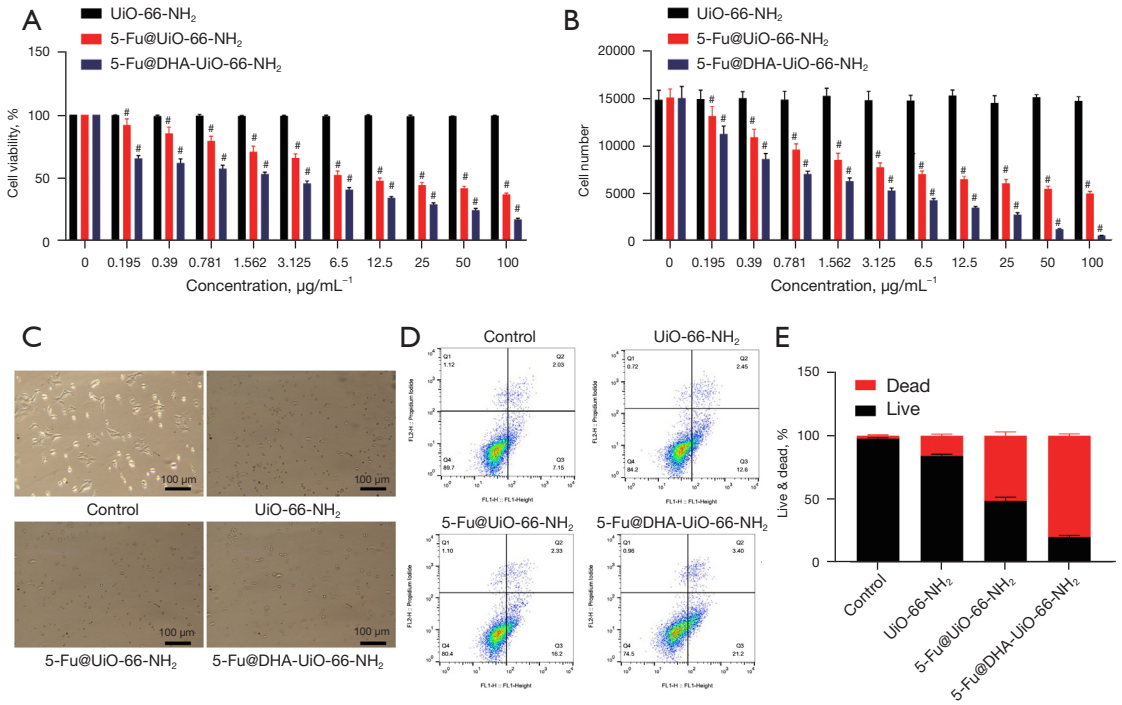

Figure 4 The effects of 5-FU@DHA-UIO-66-NH_2 on the viability and apoptosis of MCF-7 cells. (A) The effects of UIO-66-NH_2, 5-FU@UIO-66-NH_2 and 5-FU@DHA-UIO-66-NH_2 on MCF-7 cell viability; (B) the effects of UIO-66-NH_2, 5-FU@UIO-66-NH_2 and 5-FU@DHA-UIO-66-NH_2 on the number of MCF-7 cells; (C) representative images of optical microscopy detection of MCF-7 cells treated with UIO-66-NH_2, 5-FU@UIO-66-NH_2 or 5-FU@DHA-UIO-66-NH_2; (D) flow cytometry to detect the apoptosis of MCF-7 cells treated with UIO-66-NH_2, 5-FU@UIO-66-NH_2 or 5-FU@DHA-UIO-66-NH_2; (E) quantitative analysis of CLSM of MCF-7 cancer cells after incubation with UIO-66-NH_2, 5-FU@UIO-66-NH_2 or 5-FU@DHA-UIO-66-NH_2. #, P<0.05 *vs.* UIO-66-NH_2 group. Each cellular experiment was repeated three times. 5-FU, 5-fluorouracil; DHA, docosahexaenoic acid.

chemosensitivity in BC.

5-FU@DHA-UIO-66-NH2 is a safe drug-carrier for chemotherapy

Subsequently, we investigated the biosafety of 5-FU@DHA-UIO-66-NH_2 through the detection of physiological toxicity *in vivo*. Results of HE staining showed no obvious damage to the five major organs of BC mice treated by 5-FU@DHA-UIO-66-NH_2 (*Figure* 7). Then, through routine blood analysis we found that the blood parameters of the mice were in the normal range on the 1st and 7th day from 5-FU@DHA-UIO-66-NH_2 administration (*Table 1*). Furthermore, 5-FU@DHA-UIO-66-NH_2 treatment only slightly affected the level of alanine aminotransferase (ALT), alkaline phosphatase (ALP) and aspartate aminotransferase (AST) indicators, thus causing no damage to the kidney and liver (*Table 1*). In summary, 5-FU@DHA-UIO-66-NH_2 could be metabolized by BC mice and executed minimized toxic side effects on normal tissues. In this sense, 5-FU@DHA-UIO-66-NH_2 may serve as a safe drug carrier for BC treatment.

Discussion

Drug delivery systems with magnetization have attracted considerable interest for their capability of promoting the accumulation of drug at the target site (18). Especially for cancer treatment, drug loading and release based on nano-carrier with high biocompatibility and low cytotoxicity is a promising approach to improve the efficacy of conventional chemotherapy, which has long been limited by drug resistance, side effects, and low effectiveness (19). In the present study, we observed the satisfying performance of DHA-modified UIO-66-NH_2, a Zr-based MOF, when it was utilized as a carrier for 5-FU in BC treatment. We further

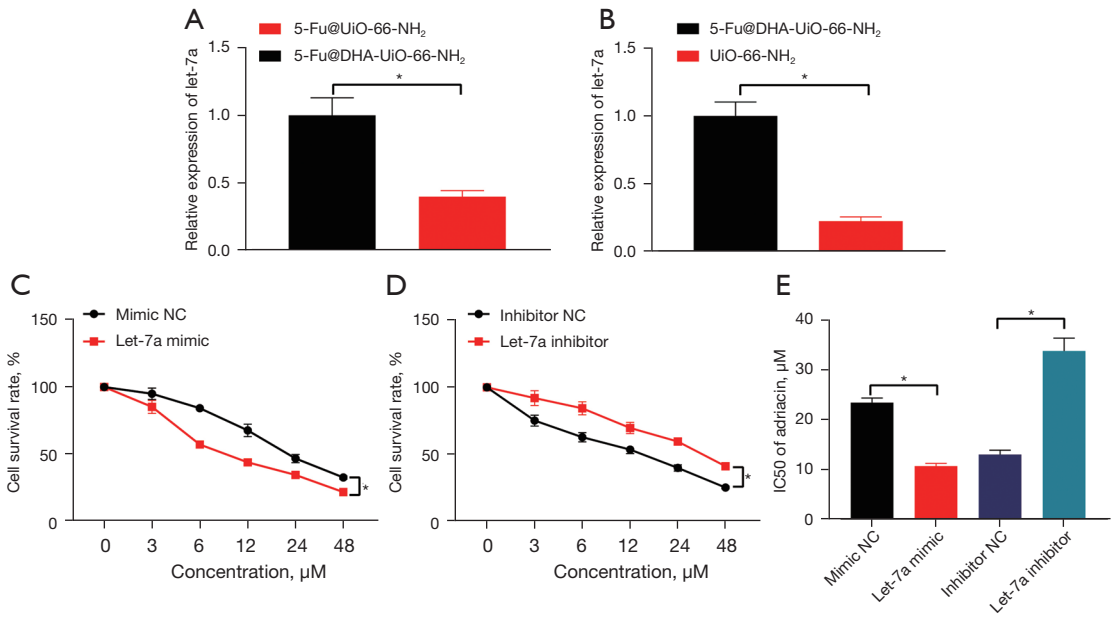

Figure 5 5-FU@DHA-UIO-66-NH_2 up-regulates let-7a to reduce the resistance of MCF-7 cells to 5-FU. (A) 5-FU@DHA-UIO-66-NH_2-induced up-regulation of let-7a in MCF-7 cells as compared with 5-FU@UIO-66-NH_2; (B) 5-FU@DHA-UIO-66-NH_2-induced up-regulation of let-7a in MCF-7 cells as compared with UIO-66-NH_2; (C) the survival rate of 5-FU-treated MCF-7/DDP cells in the presence of let-7a overexpression; (D) the survival rate of 5-FU-treated MCF-7/DDP cells in the presence of let-7a inhibition; (E) IC_{50} of 5-FU-treated MCF-7/DDP cells in response to let-7a inhibition/overexpression. *, P<0.05 between two groups. Each cellular experiment was repeated three times. 5-FU, 5-fluorouracil; DHA, docosahexaenoic acid.

illuminated that 5-FU@DHA-UIO-66-NH_2 can reduce the resistance of BC cells to 5-FU via regulation of let-7.

Initially, we successfully constructed UIO-66-NH_2 and DHA-UIO-66-NH_2 and characterized them with FT-IR, PXRD, solid-state NMR, and gas adsorption. As a member of MOFs, UIO-66-NH_2 is a crystalline material composed of inorganic zirconium ions connected by organic NH_2-H_2BDC nodes (20). Of note, UIO-66-NH_2 has been highlighted for properties such as large specific surface area and metal ions with various binding sites (8). Microorganism@UIO-66-NH_2 has been reported to be a prospective barcoding candidate for the detection of colorectal cancer-related miRNAs due to the synergy between microorganisms and UIO-66-NH_2 (21) and Fe_3O_4@UIO-66-NH_2 has been employed to develop a drug delivery system possessing sustained drug release, ideal biocompatibility, and effective therapeutic effects (7). Following previous efforts, in this study we modified UIO-66-NH_2 with DHA to deliver 5-FU, and our data unraveled that 5-FU@DHA-UIO-66-NH_2 existed stably for 24 hours in the solution of pH from 4 to 7 and possessed good water stability. Further, we substantiated that DHA-UIO-66-NH_2 could effectively load 5-FU and that the release of 5-FU against BC cells was promoted in the presence of DHA modification, especially in the weak acid microenvironment of BC tumors. Our findings corroborate prior documentation about pH-sensitive drug delivery systems, where DHA was suggested to be a promising modifier for drug delivery system in cancer treatment due to the low-pH microenvironment in cancer tissues (15,22).

Further, we substantiated that DHA-UIO-66-NH_2 and UIO-66-NH_2 particles could be effectively endocytosed by MCF-7 BC cells, while 5-FU@DHA-UIO-66-NH_2 exhibited stronger inhibiting effects on BC cell viability and stimulative effects on apoptosis as compared with 5-FU@UIO-66-NH_2. It was thus suggested that DHA increased the ability of the MOF to penetrate through the cell membrane, and 5-FU was released more effectively by DHA-modified UIO-66-NH_2. In relation to this, DHA has been identified in significant amounts in the retinal or neuronal cell membranes based on its high fluidity (23). It has also been established that DHA can affect cell or tissue physiology and function through different mechanisms, one of which is the alteration in membrane structure (24).

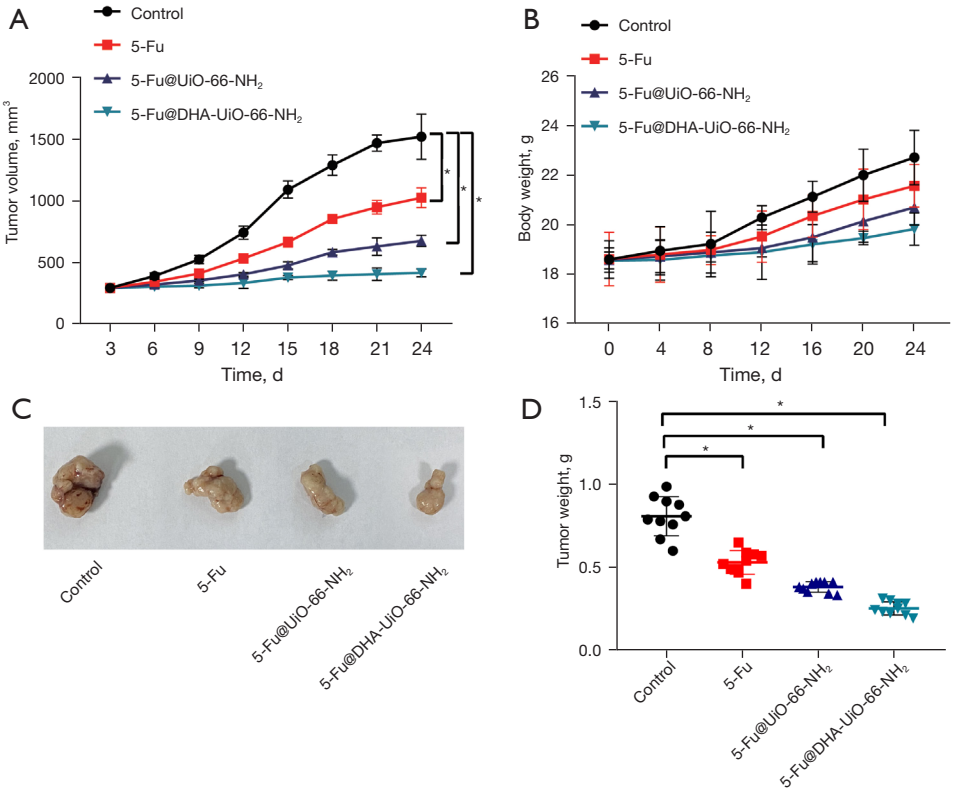

Figure 6 The effects of 5-FU@DHA-UIO-66-NH_2 on the tumorigenesis and chemosensitivity of MCF-7 cells in nude mice. (A) Tumor volume within 25 days from the intravenous injection of 5-FU, 5-FU@UIO-66-NH_2 or 5-FU@DHA-UIO-66-NH_2 in mice (*, P<0.05); (B) body weight of mice within 25 days from the intravenous injection of 5-FU, 5-FU@UIO-66-NH_2 or 5-FU@DHA-UIO-66-NH_2; (C) tumor weight 25 days after the intravenous injection of 5-FU, 5-FU@UIO-66-NH_2 or 5-FU@DHA-UIO-66-NH_2 in mice; (D) photos of xenografted tumor of mice on the 25th day after treatment with 5-FU, 5-FU@UIO-66-NH_2 or 5-FU@DHA-UIO-66-NH_2 (*, P<0.05). n=10. 5-FU, 5-fluorouracil; DHA, docosahexaenoic acid.

Table 1 Changes of blood indexes in nude mice treated with 5-FU@DHA-UIO-66-NH_2

Variables	WBC (10^9/L)	RBC (10^{12}/L)	HGB (g/L)	HCT (%)	MCV (fL)	MCH (pg)	MCHC (g/L)	PLT (10^9/L)	ALT (U/L)	ALP (U/L)	AST (U/L)
Reference range	3.91–14.93	7.48–10.91	123–167	40.5–52.9	45.8–58.1	13.5–17.2	247–361	482–1293	37–102	102–328	74–241
Healthy control	6.25±1.47	9.01±0.62	140.5±6.9	43.2±2.5	49.6±2.7	15.4±0.9	324.1±4.8	901.5±130.1	69.3±8.5	186.5±46.7	200.5±35.3
1 day after treatment	7.59±1.01	8.47±0.66	138.2±11.4	46.8±1.7	46.8±1.3	14.8±0.7	312.9±6.5	840.2±74.9	57.5±4.1	147.1±20.5	150.9±8.7
7 days after treatment	8.07±1.24	9.55±0.81	147.9±8.6	48.1±2.9	47.7±2.0	15.8±0.6	320.4±3.7	1017.8±57.3	62.6±3.9	178.4±33.1	179.6±14.2

The BC mice injected with 5-FU@DHA-UIO-66-NH_2 were euthanized on day 1 and day 7. Untreated healthy nude mice as control. Complete blood count: white blood cell (WBC), red blood cell (RBC), hemoglobin (HGB), hematocrit (HCT), mean corpuscular volume (MCV), mean corpuscular hemoglobin (MCH), mean corpuscular hemoglobin concentration (MCHC), and platelet (PLT). Serum biochemical parameters: alanine aminotransferase (ALT), alkaline phosphatase (ALP) and aspartate aminotransferase (AST).

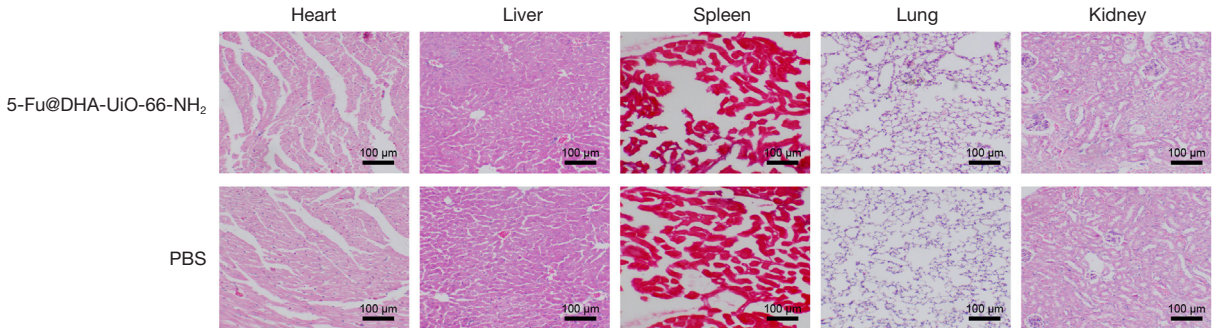

Figure 7 Observation on the damage of five major organs in nude mice after 5-FU@DHA-UIO-66-NH_2 treatment. Biosafety of 5-FU@DHA-UIO-66-NH_2 was evaluated by detecting through HE staining the damage on the major organs (heart, liver, spleen, lung, kidney) of mice that have been injected intravenously with 5-FU@DHA-UIO-66-NH_2 or PBS (n=10) seven days before. 5-FU, 5-fluorouracil; DHA, docosahexaenoic acid; PBS, phosphate buffered saline.

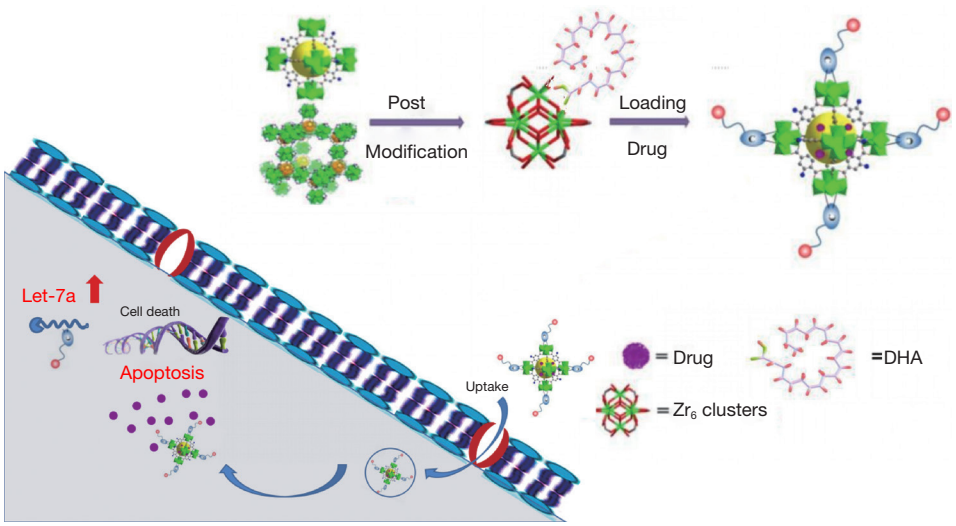

Figure 8 The mechanism graph of the regulatory role of 5-FU@DHA-UIO-66-NH_2 in BC. 5-FU@DHA-UIO-66-NH_2 up-regulated the level of let-7a to reduce the resistance of BC cells to 5-FU though inhibiting BC cell viability and promoting the apoptosis. 5-FU, 5-fluorouracil; DHA, docosahexaenoic acid; BC, breast cancer.

Subsequently, our data revealed that 5-FU@DHA-UIO-66-NH_2 up-regulated the level of miRNA let-7a to reduce the resistance of BC cells to 5-FU. In agreement with our finding, accumulating evidence has recognized let-7a as a biomarker in the management of BC, a tumor-suppressor to inhibit the proliferation of BC cells (25,26). A prior report further illuminated that DHA up-regulated the expression of let-7a and thus increase the sensitivity of BC cells to 5-FU (11). *In vivo* experiments also validated that 5-FU@DHA-UIO-66-NH_2 effectively suppressed the tumorigenic ability of BC cells and enhanced the chemosensitivity in BC mice. Moreover, we examined the biosafety of 5-FU@DHA-UIO-66-NH_2. It was revealed that 5-FU@DHA-UIO-66-NH_2 could be metabolized by BC mice and exerted minimized toxic effects on major organs and normal tissues of the mice.

Conclusions

Based on the evidence acquired, the present study elucidated that 5-FU could be effectively loaded and released by DHA-modified UIO-66-NH_2, and that 5-FU@DHA-UIO-66-NH_2, with validated biocompatibility and biosafety, up-regulated the level of let-7a to reduce the resistance of BC cells to 5-FU (*Figure 8*). By constructing 5-FU@DHA-

UIO-66-NH_2 and investigating the role of this novel drug delivery system in BC, this study characterized DHA-UIO-66-NH_2 as a promising MOF for the development of nano-targeted therapy for BC. Due to the ultrahigh surface area and porosity of MOFs, the 5-FU drug loading capacity can be greatly increased; in addition, MOFs have well-defined structure, tunable pore size, and easy chemical functionalization. When MOFs were modified with DHA, the terminal carboxyl functional group of DHA can improve the biocompatibility of MOFs and enhance the synergy with anticancer drugs (27-29). However, the MOFs used in this study still have the common problems of MOFs, such as cumbersome synthesis steps, toxic reagents needed and difficult storage.

Acknowledgments

Funding: This study was supported by Heilongjiang Provincial Natural Science Foundation of China (No. H2017048).

Footnote

Reporting Checklist: The authors have completed the ARRIVE reporting checklist. Available at https://dx.doi.org/10.21037/atm-21-5978

Data Sharing Statement: Available at https://dx.doi.org/10.21037/atm-21-5978

Conflicts of Interest: All authors have completed the ICMJE uniform disclosure form (available at https://dx.doi.org/10.21037/atm-21-5978). The authors have no conflicts of interest to declare.

Ethical Statement: The authors are accountable for all aspects of the work in ensuring that questions related to the accuracy or integrity of any part of the work are appropriately investigated and resolved. Animal experiments were approved by the Animal Ethics Committee of Harbin Medical University Cancer Hospital (approval number: 2019-185) and performed according to the Guide for the Care and Use of Laboratory animals published by the US National Institutes of Health. Extensive efforts were made to ensure minimal suffering of the animals used in the study.

References

1. Conceição F, Sousa DM, Paredes J, et al. Sympathetic activity in breast cancer and metastasis: partners in crime. Bone Res 2021;9:9.
2. Li H, Zhu S, Xu L, et al. Novel poly-β-cyclodextrin derivatives as advanced carriers for 5-fluorouracil for tumor: the impact of charge on antitumor efficiency. Transl Cancer Res 2020;9:4596-606.
3. Raj R, Mongia P, Kumar Sahu S, et al. Nanocarriers Based Anticancer Drugs: Current Scenario and Future Perceptions. Curr Drug Targets 2016;17:206-28.
4. Senapati S, Mahanta AK, Kumar S, et al. Controlled drug delivery vehicles for cancer treatment and their performance. Signal Transduct Target Ther 2018;3:7.
5. Qian Y, Khan IA, Zhao D. Electrocatalysts Derived from Metal-Organic Frameworks for Oxygen Reduction and Evolution Reactions in Aqueous Media. Small 2017.
6. Saura-Sanmartin A, Martinez-Cuezva A, Marin-Luna M, et al. Effective Encapsulation of C60 by Metal-Organic Frameworks with Polyamide Macrocyclic Linkers. Angew Chem Int Ed Engl 2021;60:10814-9.
7. Xue Z, Zhu M, Dong Y, et al. An integrated targeting drug delivery system based on the hybridization of graphdiyne and MOFs for visualized cancer therapy. Nanoscale 2019;11:11709-18.
8. Gao X, Cui R, Ji G, et al. Size and surface controllable metal-organic frameworks (MOFs) for fluorescence imaging and cancer therapy. Nanoscale 2018;10:6205-11.
9. Hao L, Lin L, Zhou J. pH-Responsive Zwitterionic Copolymer DHA-PBLG-PCB for Targeted Drug Delivery: A Computer Simulation Study. Langmuir 2019;35:1944-53.
10. Luo Z, Jiang J. pH-sensitive drug loading/releasing in amphiphilic copolymer PAE-PEG: integrating molecular dynamics and dissipative particle dynamics simulations. J Control Release 2012;162:185-93.
11. Abazari R, Mahjoub AR, Ataei F, et al. Chitosan Immobilization on Bio-MOF Nanostructures: A Biocompatible pH-Responsive Nanocarrier for

Doxorubicin Release on MCF-7 Cell Lines of Human Breast Cancer. Inorg Chem 2018;57:13364-79.
12. Hannafon BN, Carpenter KJ, Berry WL, et al. Exosome-mediated microRNA signaling from breast cancer cells is altered by the anti-angiogenesis agent docosahexaenoic acid (DHA). Mol Cancer 2015;14:133.
13. Shah MY, Pan X, Fix LN, et al. 5-Fluorouracil drug alters the microRNA expression profiles in MCF-7 breast cancer cells. J Cell Physiol 2011;226:1868-78.
14. Mi Y, Liu F, Liang X, et al. Tumor suppressor let-7a inhibits breast cancer cell proliferation, migration and invasion by targeting MAGE-A1. Neoplasma 2019;66:54-62.
15. Gao GH, Li Y, Lee DS. Environmental pH-sensitive polymeric micelles for cancer diagnosis and targeted therapy. J Control Release 2013;169:180-4.
16. Li H, Li X, Shi X, et al. Effects of magnetic dihydroartemisinin nano-liposome in inhibiting the proliferation of head and neck squamous cell carcinomas. Phytomedicine 2019;56:215-28.
17. Hashemi-Moghaddam H, Kazemi-Bagsangani S, Jamili M, et al. Evaluation of magnetic nanoparticles coated by 5-fluorouracil imprinted polymer for controlled drug delivery in mouse breast cancer model. Int J Pharm 2016;497:228-38.
18. Zhou Z, Vázquez-González M, Willner I. Stimuli-responsive metal-organic framework nanoparticles for controlled drug delivery and medical applications. Chem Soc Rev 2021;50:4541-63.
19. Chen K, Qian Y, Wang C, et al. Tumor microenvironment-responsive, high internal phase Pickering emulsions stabilized by lignin/chitosan oligosaccharide particles for synergistic cancer therapy. J Colloid Interface Sci 2021;591:352-62.
20. Tang J, Chen Y, Zhao M, et al. Phenylthiosemicarbazide-functionalized UiO-66-NH2 as highly efficient adsorbent for the selective removal of lead from aqueous solutions. J Hazard Mater 2021;413:125278.
21. Xiang Y, Yan H, Zheng B, et al. Microorganism@UiO-66-NH2 Composites for the Detection of Multiple Colorectal Cancer-Related microRNAs with Flow Cytometry. Anal Chem 2020;92:12338-46.
22. Wang D, Zhou J, Chen R, et al. Magnetically guided delivery of DHA and Fe ions for enhanced cancer therapy based on pH-responsive degradation of DHA-loaded Fe3O4@C@MIL-100(Fe) nanoparticles. Biomaterials 2016;107:88-101.
23. Cardoso C, Afonso C, Bandarra NM. Dietary DHA and health: cognitive function ageing. Nutr Res Rev 2016;29:281-94.
24. Calder PC. Docosahexaenoic Acid. Ann Nutr Metab 2016;69 Suppl 1:7-21.
25. Khalighfard S, Alizadeh AM, Irani S, et al. Plasma miR-21, miR-155, miR-10b, and Let-7a as the potential biomarkers for the monitoring of breast cancer patients. Sci Rep 2018;8:17981.
26. Du J, Fan JJ, Dong C, et al. Inhibition effect of exosomes-mediated Let-7a on the development and metastasis of triple negative breast cancer by down-regulating the expression of c-Myc. Eur Rev Med Pharmacol Sci 2019;23:5301-14.
27. Tong PH, Zhu L, Zang Y, et al. Metal-organic frameworks (MOFs) as host materials for the enhanced delivery of biomacromolecular therapeutics. Chem Commun (Camb) 2021;57:12098-110.
28. Zheng Y, Zhang X, Su Z. Design of metal-organic framework composites in anti-cancer therapies. Nanoscale 2021;13:12102-18.
29. Sun Y, Zheng L, Yang Y, et al. Metal-Organic Framework Nanocarriers for Drug Delivery in Biomedical Applications. Nanomicro Lett 2020;12:103.

(English Language Editor: B. Meiser)

Cite this article as: Li J, Lu F, Shao X, You B. 5-FU@DHA-UIO-66-NH_2 potentiates chemotherapy sensitivity of breast cancer cells through a microRNA let-7a-dependent mechanism. Ann Transl Med 2021;9(24):1761. doi: 10.21037/atm-21-5978

Supplementary

Table S1 Recreation system for miRNA reverse transcription

Reagent	Volume (μL)
2*miRNA Reaction Buffer	10
miRNA RT Enzyme Mix	2
Total RNA	1
Rnase-free H_2O	Up to 20

Table S2 First recreation system for mRNA reverse transcription

Reagent	Volume (μL)
Oligo	1
RNA	2
Rnase-free-H_2O	Up to 12

Table S3 Second recreation system for mRNA reverse transcription

Reagent	Volume (μL)
dNTP	2
RT	1
RI	1
5*Reaction Buffer	4

Table S4 PCR primer sequences

Gene	Sequence (5'-3')
let-7a	RT: GTCGTATCCAGTGCAGGGTCCGAGGTATTCGCAC TGGATACGACAACTAT Forward: TCGGCGTGAGGTAGTAGGTTGT Reverse: GTCGTATCCAGTGCAGGGTCCGAGGT
U6	RT: AAAATATGGAACGCTTCACGAATTTG Forward: CTCGCTTCGGCAGCACATATACT Reverse: ACGCTTCACGAATTTGCGTGTC

Table S5 Recreation system for PCR

Reagent	Volume(μL)
2*miRcute Plus miRNA Premix	10
Reverse Primer (10 μM)	0.4
Forward Primer (10 μM)	0.4
cDNA	1
Rnase-free-H_2O	Up to 20

https://dx.doi.org/10.21037/atm-21-5978